Supporting Information

Methylated Precursor Leads to Carbon Nitride (CN_x) With Improved Interfacial Interactions for Enhanced Photocatalytic Performance

Peter Osei Ohemeng,[a] and Robert Godin*[a,b,c]

[a]*Department of Chemistry, The University of British Columbia, Kelowna, BC V1V 1V7, Canada*

[b]*Clean Energy Research Center, University of British Columbia, 2360 East Mall, Vancouver, BC, V6T 1Z3, Canada*

[c]*Okanagan Institute for Biodiversity, Resilience, and Ecosystem Services, University of British Columbia, Kelowna, BC, Canada*

Corresponding author email: robert.godin@ubc.ca

Table of Contents

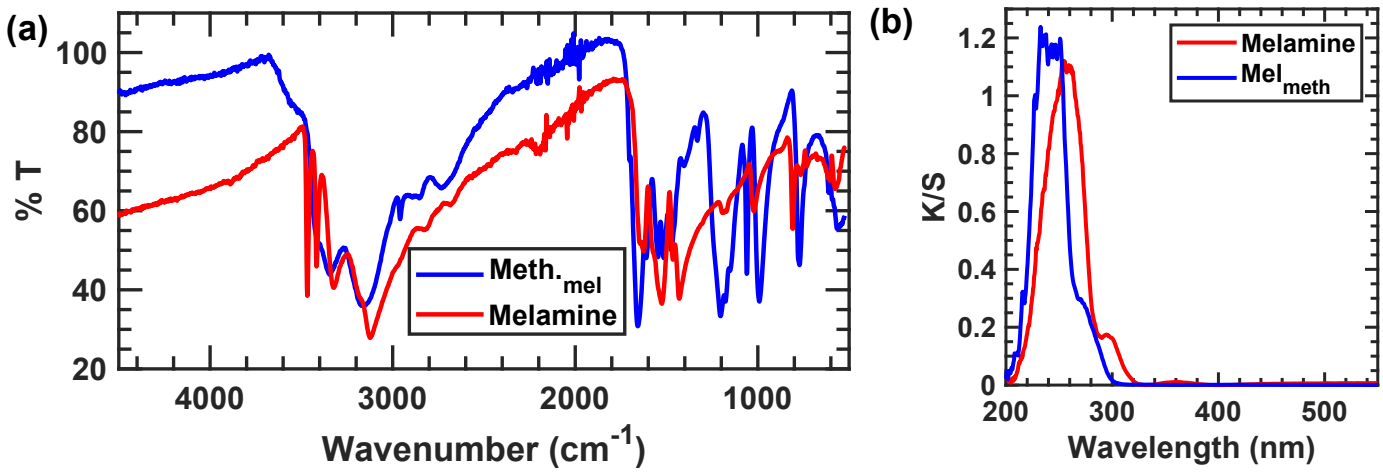

Figure S1.(a) FTIR spectra of Mel_{meth} and Melamine. (b) UV-vis DRS spectra of Mel_{meth} and Melamine.

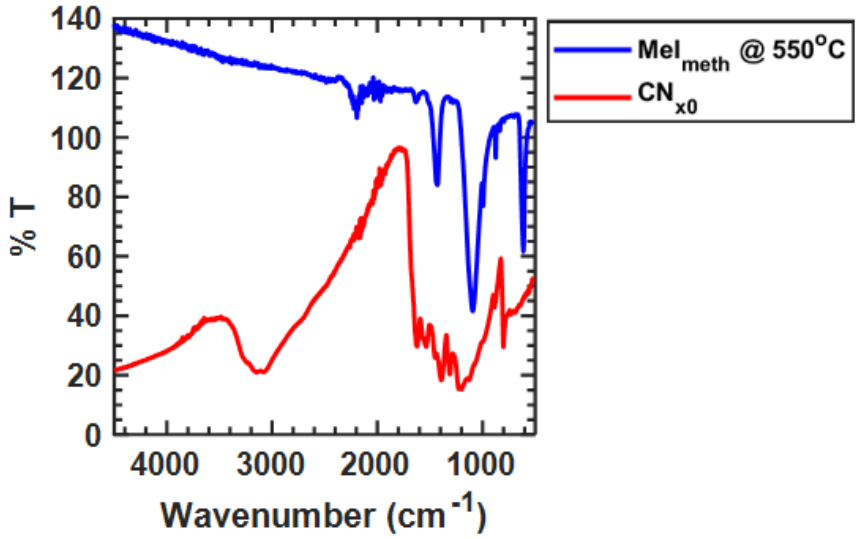

Figure S2. FTIR spectra of Mel_{meth} heated at 550 °C for 4 hours (ramp rate = 2 °C min^{-1}) and CN_{x0}

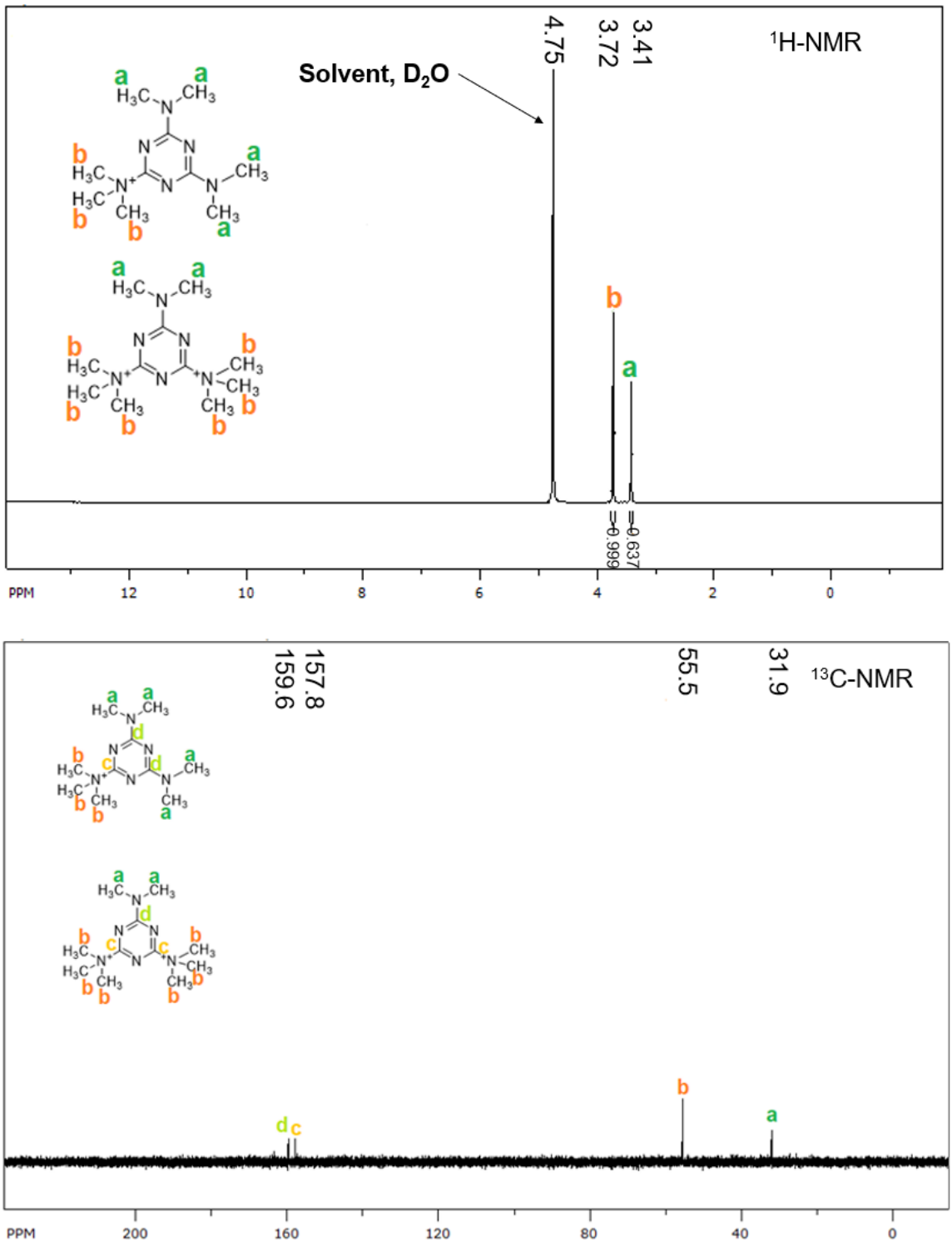

Figure S3. ^{1}H-NMR of Mel_{meth} (Top) and ^{13}C-NMR of Mel_{meth} (bottom) taken in D_2O solvent. Inset is the elucidated structure based on NMR signals.

High-Performance Liquid Chromatography (HPLC)

The chromatographic separation and detection of melamine and the Mel_{meth} product was achieved with a Waters HPLC system with a conductivity detector in an isocratic mode. The samples were analyzed on a Symmetry C18 column (75 × 4.6 mm I.D., 3.5 µm). The mobile phase used was HPLC grade water (100 %), and the flow rate was 0.3 $mLmin^{-1}$ for 6 minutes. The injection volume was 20 µL and the working sample concentration was 100 µg mL^{-1}.

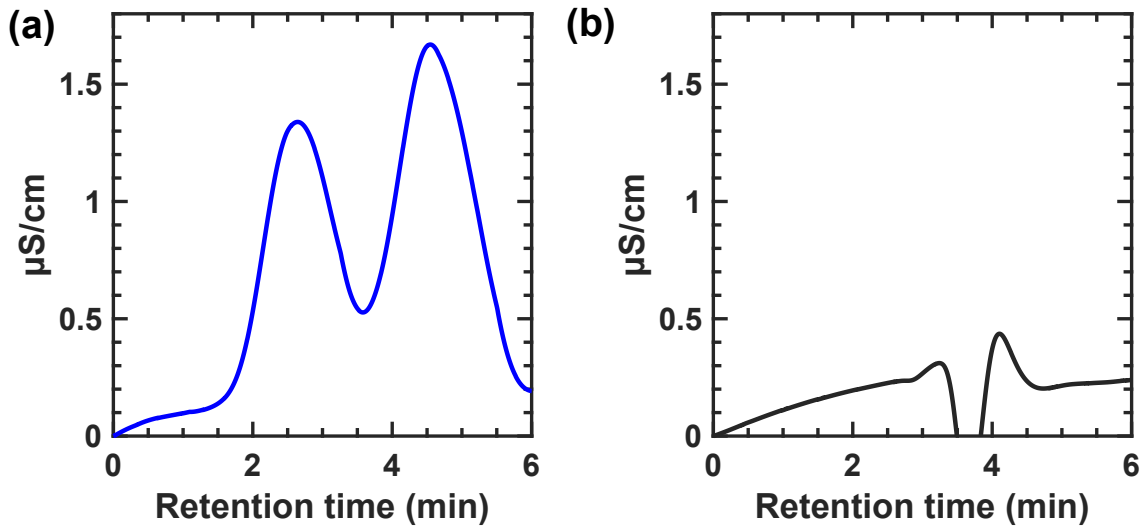

Figure S4. HPLC-conductivity chromatogram of (a) Mel_{meth} product and (b) Melamine. Chromatographic conditions: HPLC-grade water (eluent), 0.3 mL min^{-1}(flow rate), 20 µL (injection volume). Separation was achieved under ambient conditions.

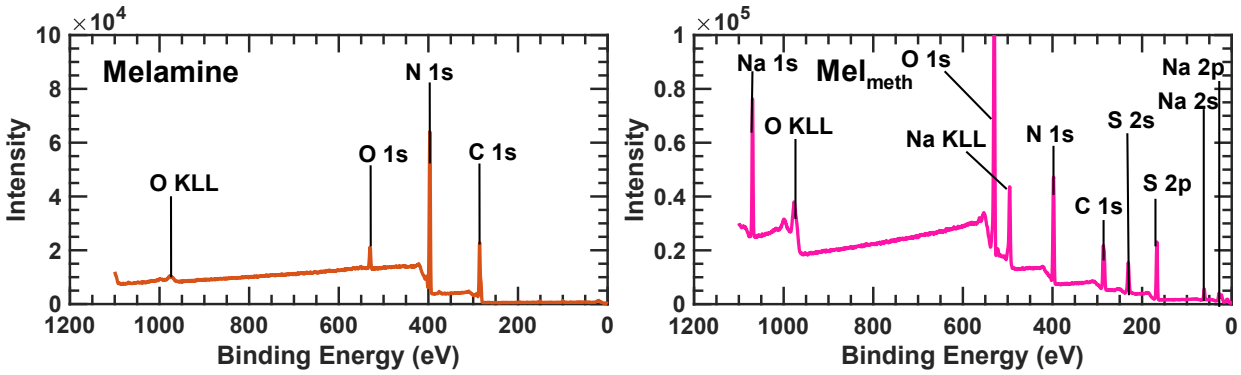

Figure S5. Survey XPS spectra of the precursors and their assignments. The additional peaks in the spectrum of Mel_{meth} is due to our synthetic approach.

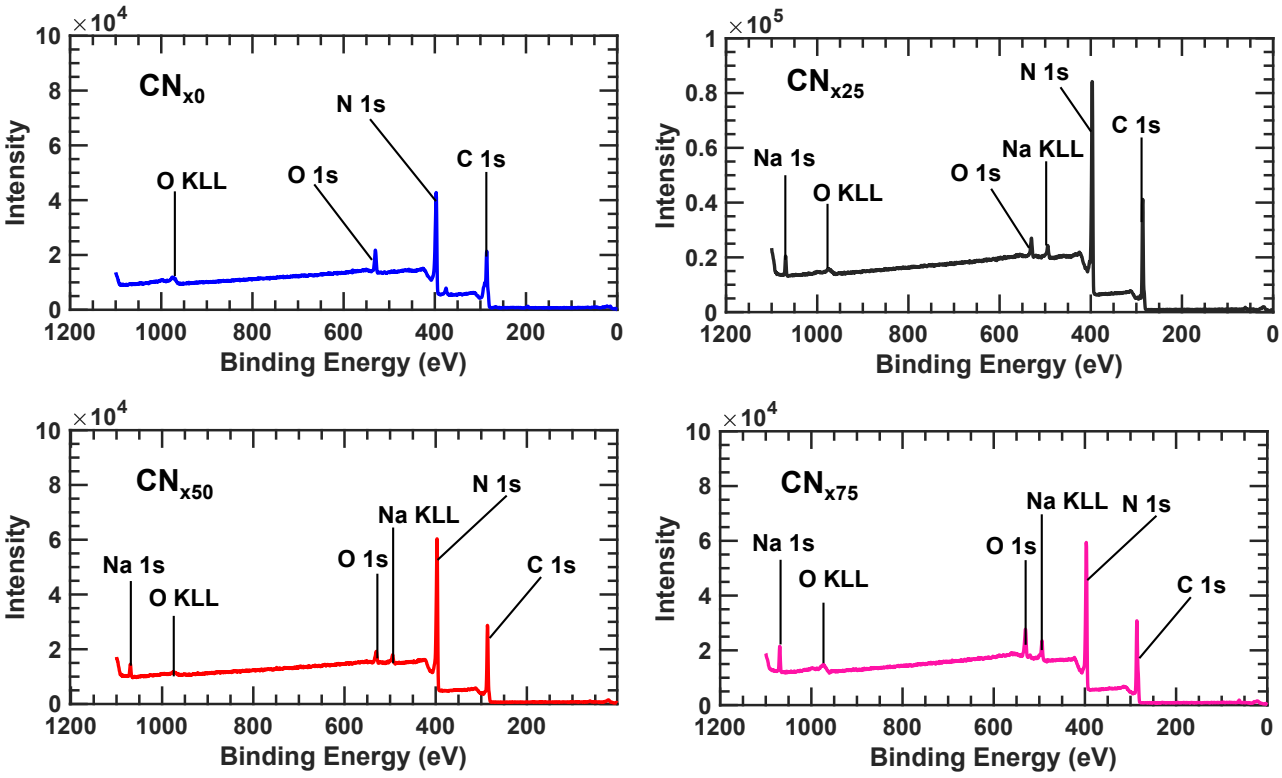

Figure S6. Survey XPS spectra of all samples and their assignments.

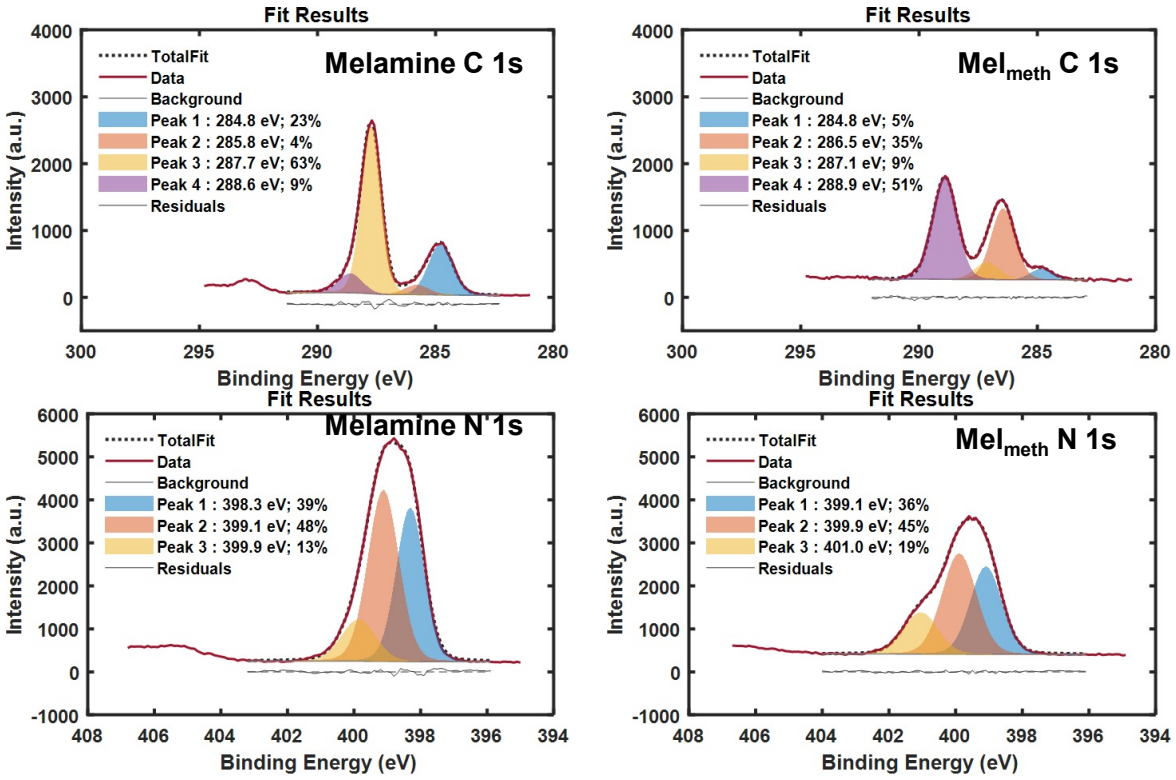

Figure S7: C 1s and N 1s XPS spectra of Melamine and Mel_{meth}. The C 1s and N 1s spectra have been deconvoluted into four and three main peaks respectively by means of a Shirley background and Voigt peaks with FWHM of 1.1 eV ± 10 %. The binding energy values have been shifted to the reference value of 284.8 eV for peak 4 in the C 1s spectra corresponding to adventitious C-C environments. The corresponding binding energy shifts have been applied to the N 1s spectra.

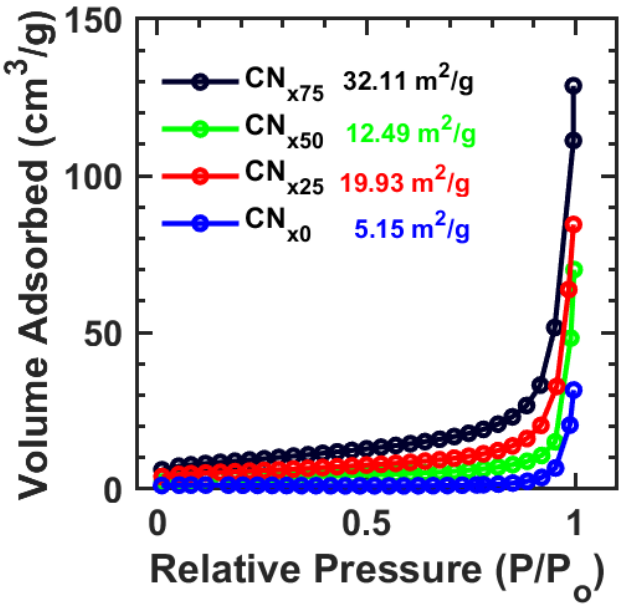

Figure S8. N_2 adsorption-desorption isotherm of samples.

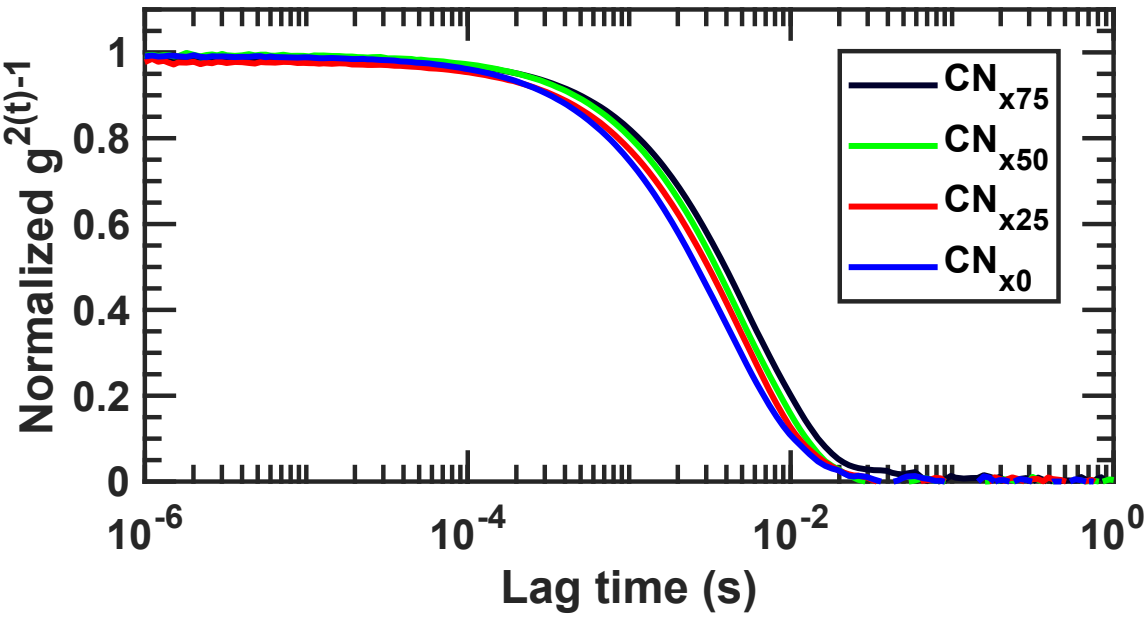

Figure S9. Normalized dynamic light scattering (DLS) correlation curve of samples for particle size determination. Data was acquired in aqueous media and at 90 ° scattering angle.

Table S1. Summary of particle size distribution determined by CONTIN analysis[2] of the DLS correlation traces shown in **Figure S9**. The main particle population of each sample is bolded.

Sample	Size (nm)	Relative Amount (%)
CN_{x0}	17.48	1.3
	317.17	**98.7**
CN_{x25}	22.82	1.5
	362.03	**93.4**
	5687.80	5.1
CN_{x50}	58.28	4.3
	381.16	**95.7**
CN_{x75}	33.12	1.0
	382.43	**88.0**
	56020	11.0

Direct and Indirect Bandgap Determination

The direct and indirect bandgap energies for the samples were determined by constructing a Tauc plot for each sample based on their Kubelka-Munk transform dataset, utilizing a MATLAB application which is based on the multivariate adaptive regression splines (MARS) algorithm. Basically, the method divides the non-linear absorption plot into several linear segments that approximately fit the signal and takes the segment with the largest weight as the optimal line segment for predicting the bandgap[1]. The bandgap is taken as the intercept of this linear segment with the linear baseline found at low energies.

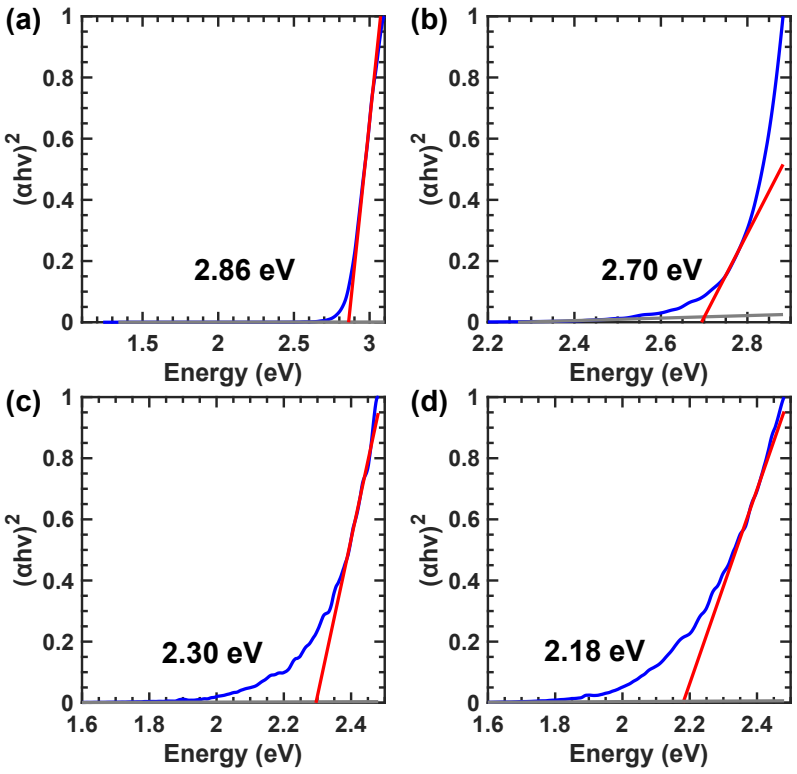

Figure S10. Tauc plots and line of fit (red line) used to determine the direct bandgap energy of: (a) CN_{x0} (b) CN_{x25} (c) CN_{50} and (d) CN_{x75}.The extracted band gap is the intersection of the fit with the y = 0 line (gray line) and is quoted at the bottom right corner of each graph.

Table S2. Indirect and Direct bandgap energies of Modified and Benchmark CN_x samples

Sample	Indirect Bandgap Energy (eV)	Direct Bandgap Energy (eV)
CN_{x0}	2.67	2.86
CN_{x25}	2.60	2.70
CN_{x50}	1.85	2.30
CN_{x75}	1.78	2.18

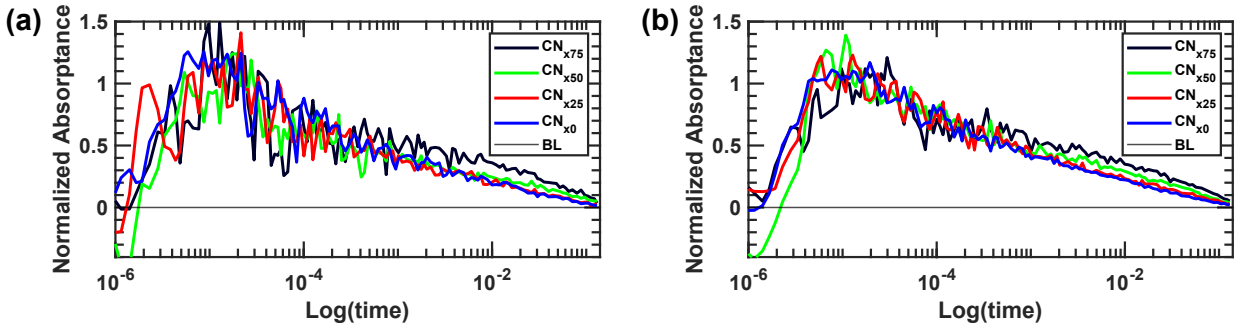

Figure S11. TAS decay kinetics of samples normalized at 20 μs and monitored at (a) 800 nm and (b) 850 nm. The excitation pulse used was 355 nm excitation (100 μJcm^{-2}) and the y = 0 line is indicated as BL in legend.

Table S3. Compilation of α values of all samples extracted from the slope of the log-log fitting of the TAS decay kinetics at 800 nm, 850 nm, and 900 nm.

Sample	800 nm	850 nm	900 nm
CN_{x0}	0.25	0.27	0.25
CN_{x25}	0.24	0.26	0.24
CN_{x50}	0.19	0.21	0.20
CN_{x75}	0.17	0.15	0.16

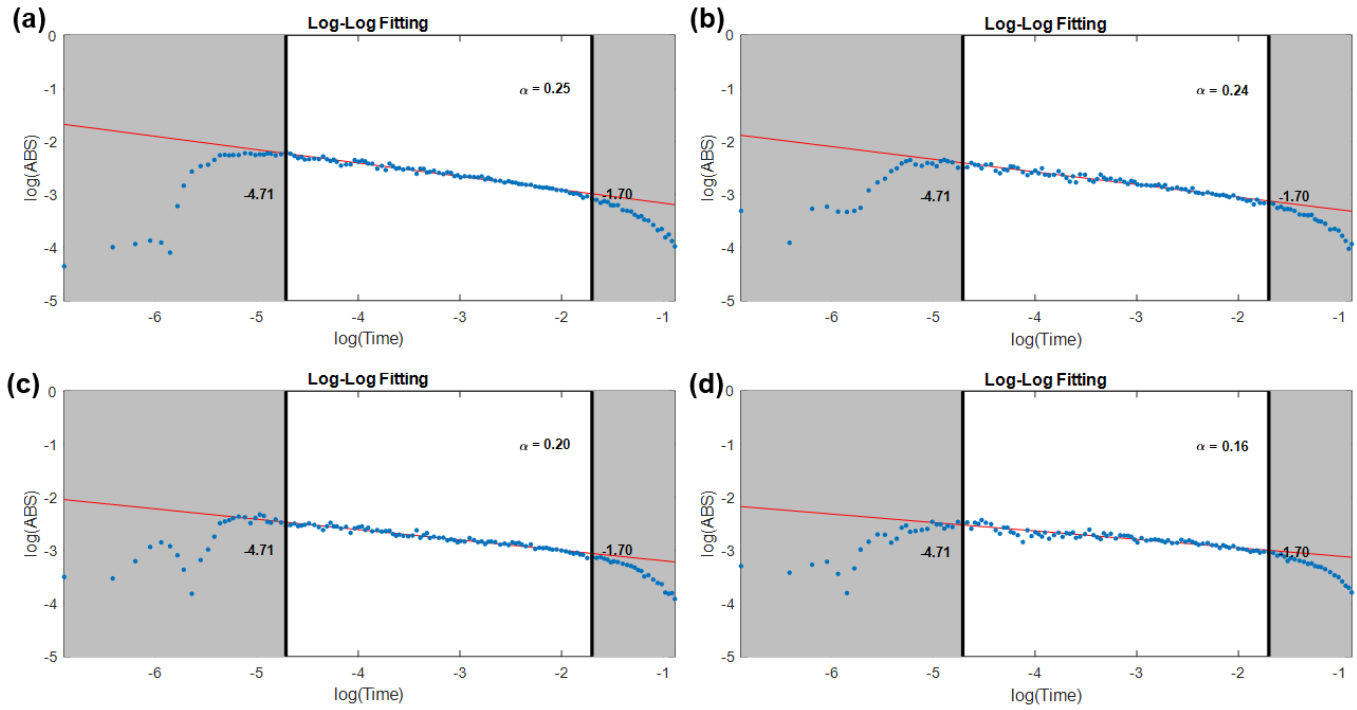

Figure S12. The log-log plots of the TAS decay kinetics at 900 nm of (a) CN_{x0} (b) CN_{x25} (c) CN_{x50} and (d) CN_{x75}

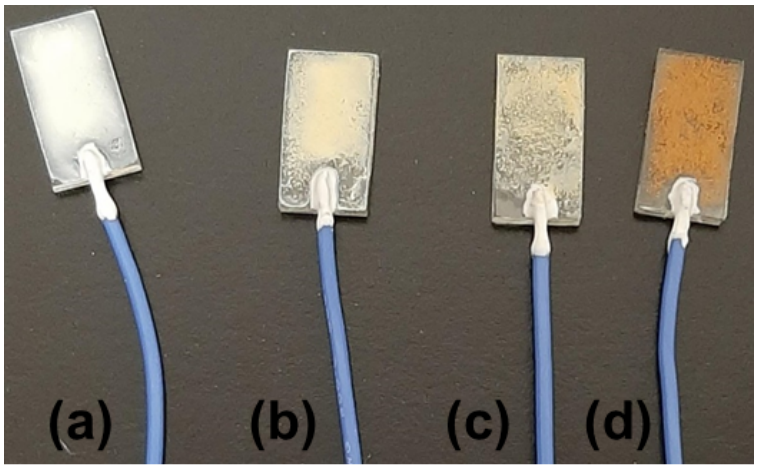

Figure S13. Pictures of photoelectrodes prepared by spreading 50 µL of 20 mg/mL CN_{xy} suspension. (a) CN_{x0} (b) CN_{x25} (c) CN_{x50} and (d) CN_{x75}

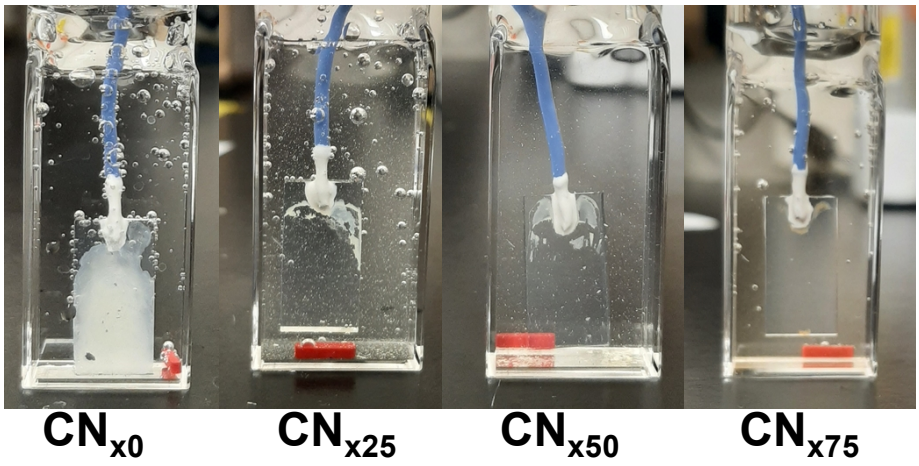

Figure S14. Pictures of CN_{xy} photoelectrodes suspended into 0.1 M Na_2SO_4 electrolyte. Pictures were taken immediately after suspending photoelectrodes into electrolyte. Bubbles were formed as electrolyte solution was ejected from a syringe to fill the cuvette.

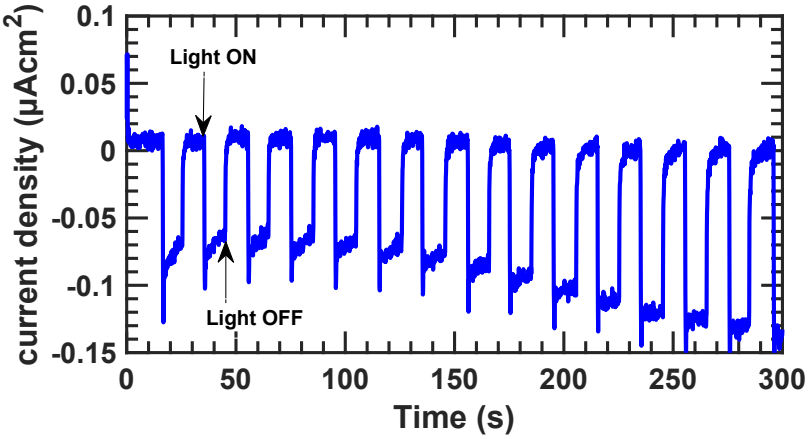

Figure S15. Photocurrent measurement of CN_{x0} in 0.1 M Na_2SO_4. Light source is 405 nm LED and was switched on and off within 10 s intervals. The sharp peaks are owed to charge recombination.

Apparent Quantum Yield (AQY) Calculation

The AQY was determined for each sample as follows. Firstly, the energy of a photon from 405 nm light was calculated.

$$E_t = \frac{hc}{\lambda} = \frac{(6.63 \times 10^{-34} \frac{m^2 kg}{s}) \times (2.998 \times 10^{8} \frac{m}{s})}{4.05 \times 10^{-7} m} = 4.90 \times 10^{-19} \frac{J}{photon}$$

Afterwards, the total energy per second was calculated from the power density of the light

$$E_t = P * Area = (10.0 \frac{mW}{cm^2} \times 2\ cm^2)/1000 = 0.02 \frac{J}{s}$$

This is followed by the calculation of the total number of photons

$$I = \frac{0.02 \frac{J}{s}}{4.90 \times 10^{-19} \frac{J}{photon}} = 4.08 \times 10^{16} \frac{photons}{s}$$

The AQY was then calculated as

$$AQY = \frac{nR}{I}$$

Where R is the rate of hydrogen evolution in μmols^{-1} and n is the number of mols needed for the reaction, which in this case is 2 for proton reduction and I is the total number of photons hitting the samples per second.

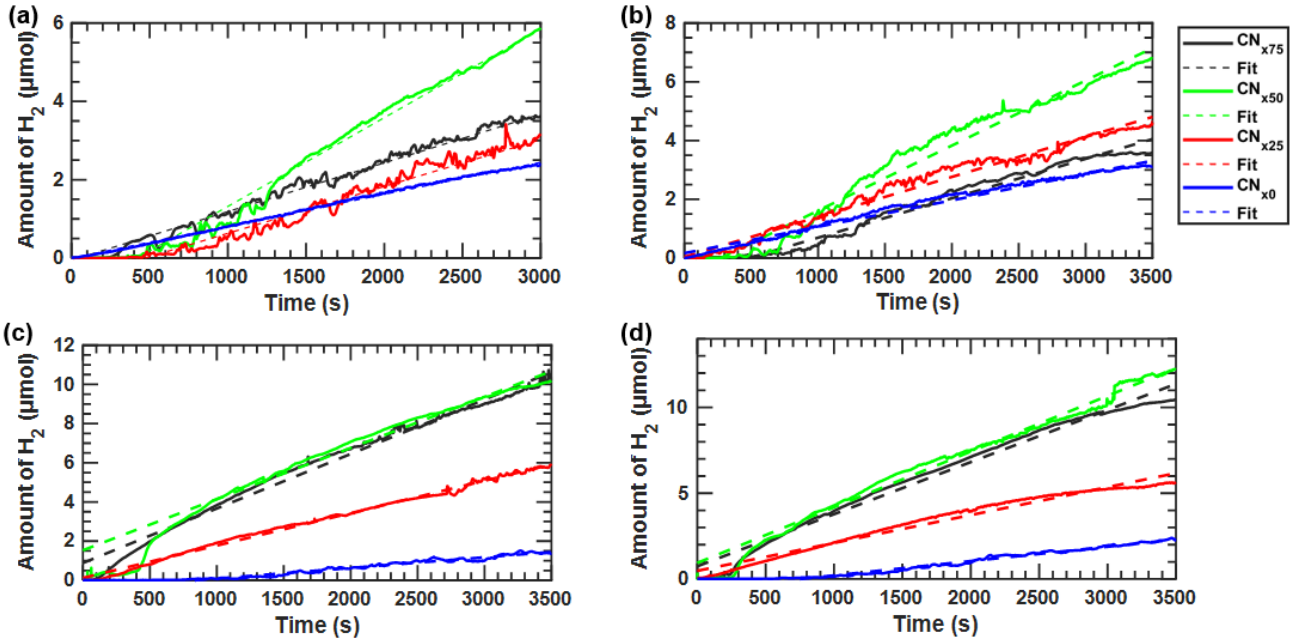

Figure S16. H_2 production over time after excitation with a 405 nm LED. (a) Trial 1 (b) Trial 2 (c) Trial 3 and (d) Trial 4. The linear range was used to determine the slope and rate of H_2 production.

Table S4. Mean slope of all HER trials and standard deviation reported with the calculated AQY. Slope values are reported in μmol s^{-1}.

Sample	HER 1 Slope	HER 2 Slope	HER 3 Slope	HER 4 Slope	Mean	Std. Dev.	AQY (%)
CN_{x0}	0.0008	0.0009	0.0005	0.0008	0.0008	0.0002	2.4
CN_{x25}	0.0013	0.0014	0.0017	0.0016	0.0015	0.0002	4.4
CN_{x50}	0.0023	0.0022	0.0026	0.0032	0.0026	0.0005	7.7
CN_{x75}	0.0012	0.0014	0.0028	0.0030	0.0021	0.0009	6.2

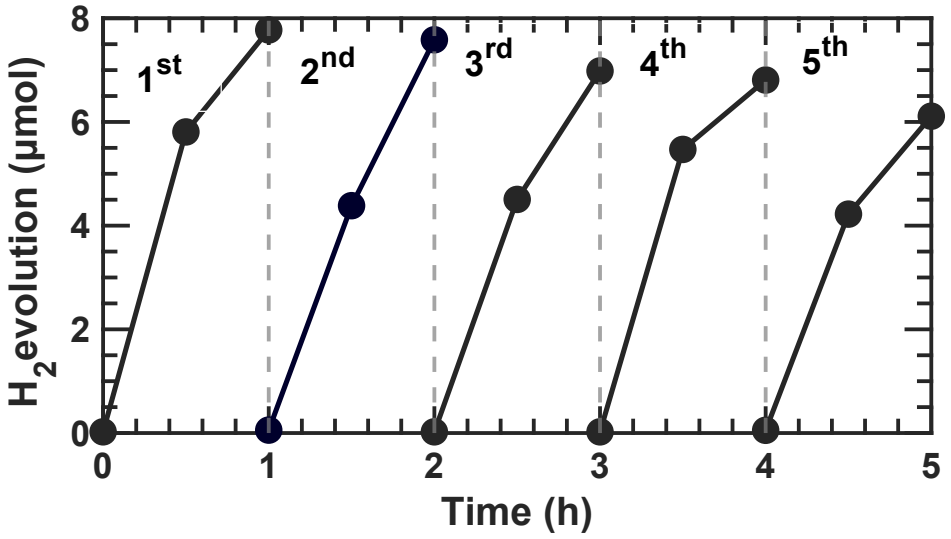

Figure S17. Cyclic stability test of CN_{x50}. The sample cell was purged with Argon to remove the H_2 in between each cycle.

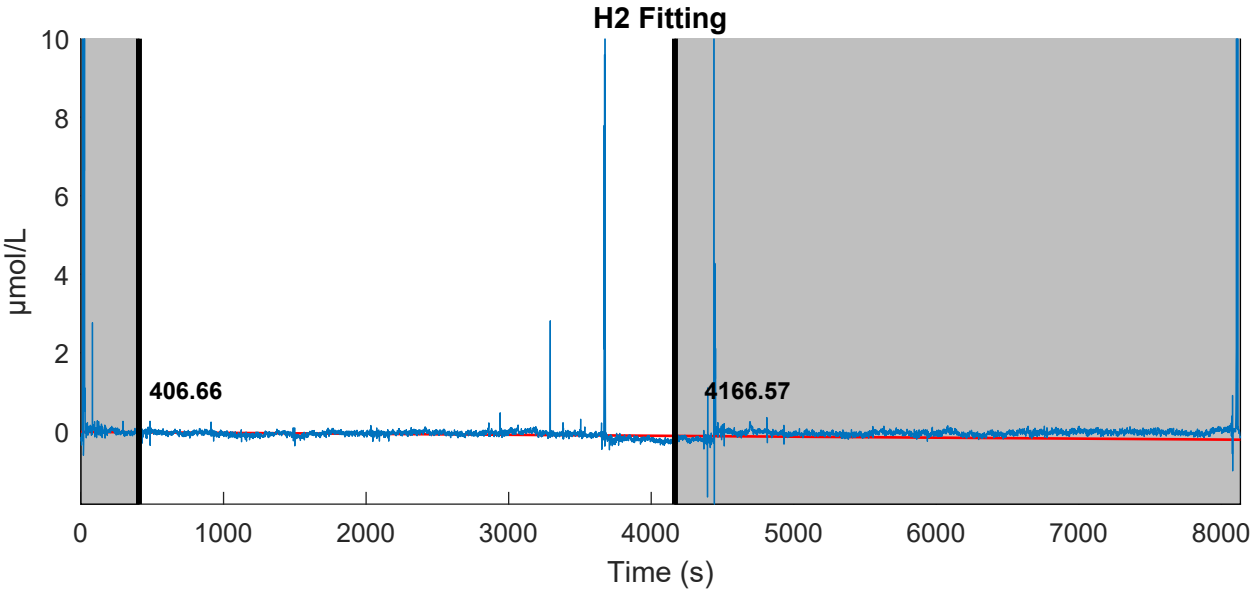

Figure S18. H_2 production on CN_{x75} over time after excitation with a 660 nm LED.

Figure S19. HER plots of CN_{x50} with photodeposited Pt as cocatalyst. (a) without sonication of suspension prior to photodeposition and (b) with sonication of suspension prior to photodeposition.

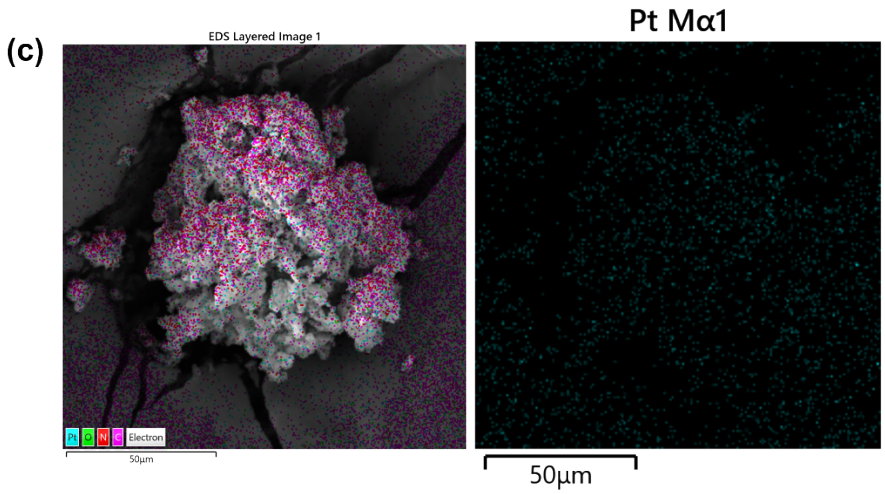

Figure S20. SEM-EDS map of Pt deposited CN_{x50} after HER. Dispersion was sonicated prior to Pt photodeposition.

Adsorption Capacity and Dye Degradation Efficiency Calculation

The adsorption capacities of the photocatalysts and the percent degradation of RhB dye by the various photocatalysts were calculated by adopting the equations below

$$Adsorption\ capacity = \frac{(C_o - C_e)V}{W}$$

Where C_o is the initial RhB dye concentration, C_e is the concentration of RhB after equilibrium, V is the volume of RhB dye solution, and W is the mass of photocatalyst.

$$Percent\ degradation = \frac{(C_o - C)}{C_o} \times 100$$

Where C_o is the initial RhB dye concentration and C is the final RhB dye concentration after 180 minutes of visible light irradiation in the presence of the photocatalyst.

Table S5. The quantitative values of the dye degradation efficiency of RhB by the individual samples and the first order rate constants, *k* of all samples taken as slope of linear fitting to the experimental data of $\ln(C/C_o)$ vs Time (min) shown in **Figure 7e**, and their corresponding R^2 values.

Sample	Adsorption Capacity (mg/g)	Dye Degradation Efficiency (%)	Normalized Dye Degradation Efficiency	First Order Rate Constant, *k* (min^{-1})	R^2
CN_{x0}	0.6	19.7	1	1.2×10^{-3}	0.955
CN_{x25}	0.6	53.0	2.7	4.5×10^{-3}	0.980
CN_{x50}	0.6	54.0	2.7	4.0×10^{-3}	0.919
CN_{x75}	1.1	61.0	3.1	5.0×10^{-3}	0.876

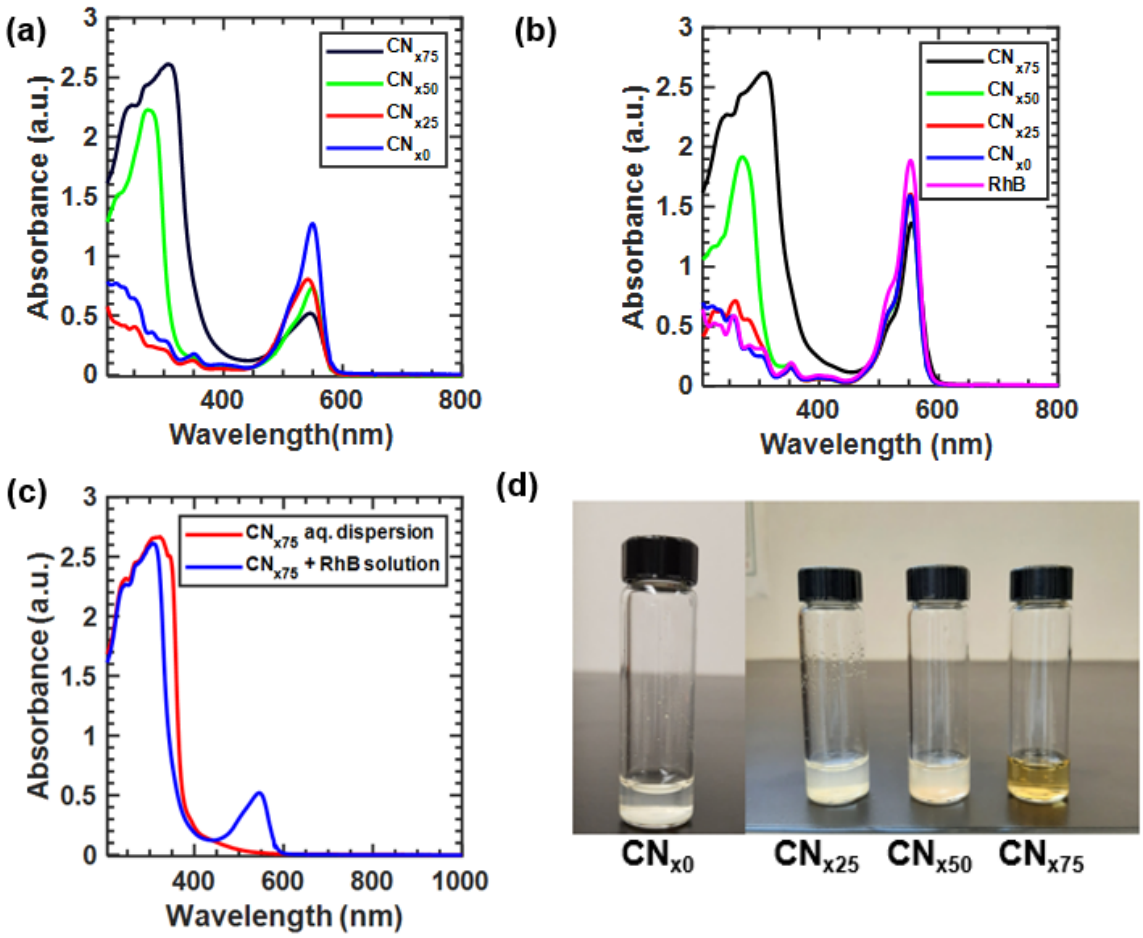

Figure S21. (a) UV-vis spectra of the photodegradation of RhB by photocatalysts after 180 minutes of light irradiation. (b) UV-vis spectra of RhB solution charged with photocatalyst following equilibration under dark conditions for 60 minutes. The spectrum of the pre-equilibrated solution (10 mg L^{-1} RhB solution) is labelled as RhB (magenta trace) in legend. The spectra describe the adsorption capacities of the individual photocatalysts. (c) UV-vis spectra of CN_{x75} dispersion in water and RhB solution charged with CN_{x75} after 180 minutes of light irradiation. (RhB solution = 10 mg L^{-1}). (d) Aqueous dispersions of samples after 2 hours of sitting without agitation.

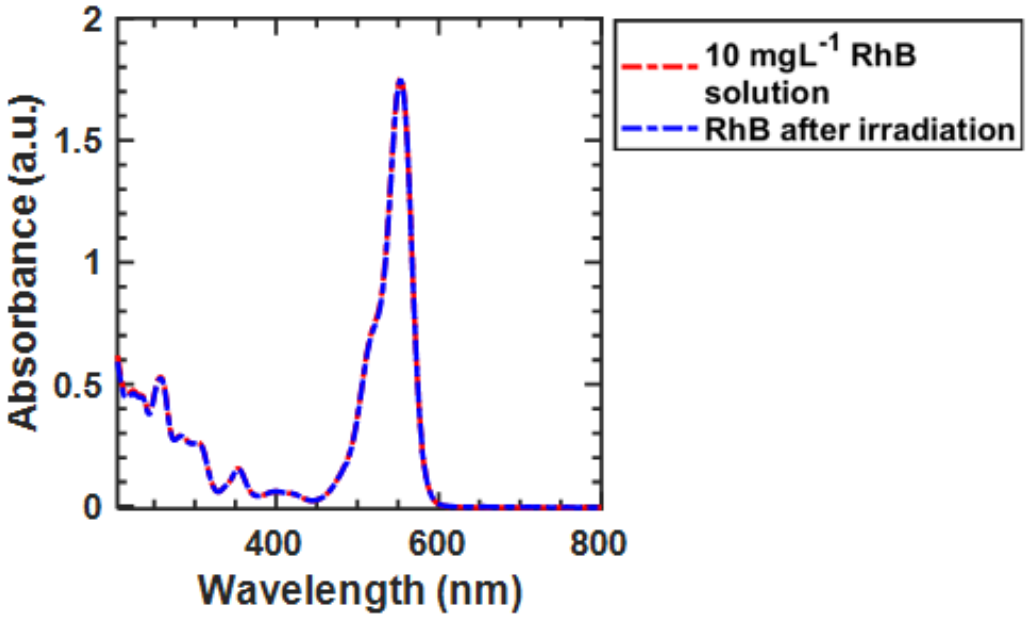

Figure S22. Control experiment of RhB dye degradation. Absorption spectra of 10 mg L^{-1} RhB dye solution (red) and 10 mg L^{-1} RhB dye solution after 180 minutes of light irradiation (wavelength = 405 nm and irradiation power = 10 mW cm^{-2}).w

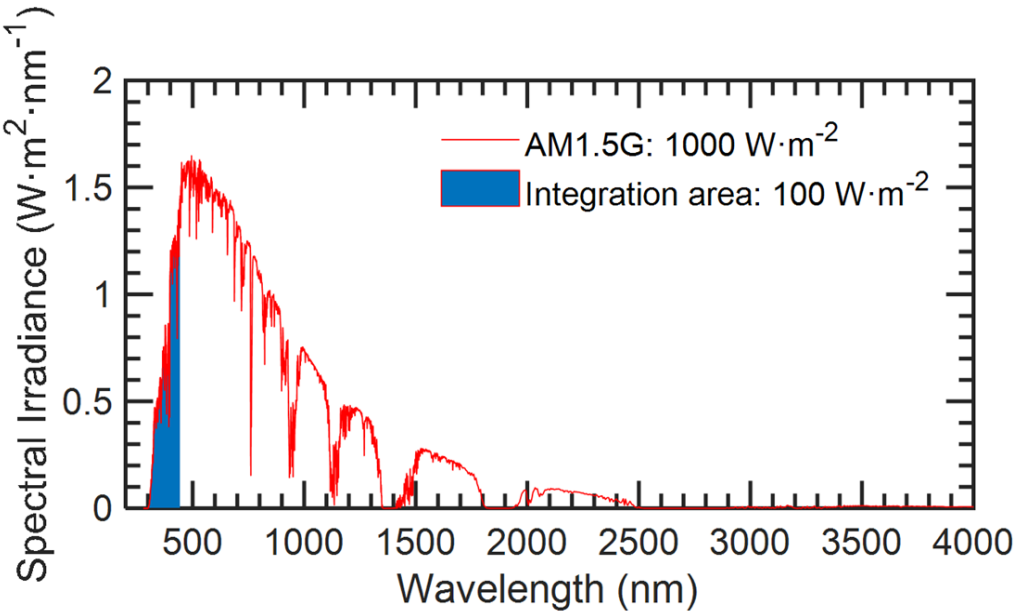

Figure S23. AM1.5G and the integration of spectral region from 280 nm to ca. 450 nm. The blue area corresponds to the amount of solar irradiation absorbed by CN_x under the sunlight.

References

(1) Schwarting, M.; Siol, S.; Talley, K.; Zakutayev, A.; Phillips, C. Automated Algorithms for Band Gap Analysis from Optical Absorption Spectra. *Mater. Discov.* **2017**, *10*, 43–52. https://doi.org/10.1016/j.md.2018.04.003.

(2) Stetefeld, J.; McKenna, S. A.; Patel, T. R. Dynamic Light Scattering: A Practical Guide and Applications in Biomedical Sciences. *Biophys. Rev.* **2016**, *8* (4), 409–427. https://doi.org/10.1007/s12551-016-0218-6.